第 54 卷第 2 期
2026 年 2 月

硅 酸 盐 学 报
JOURNAL OF THE CHINESE CERAMIC SOCIETY

Vol. 54，No. 2
February，2026

http://jccsoc.cbpt.cnki.net

DOI：10.14062/j.issn.0454-5648.20250658

基于声发射的高原大温差环境桥墩混凝土开裂机理

董昊良[1,2]，李化建[1,2]，杨志强[1,2]，黄法礼[1,2]

(1. 中国铁道科学研究院集团有限公司铁道建筑研究所，北京 100081；2. 高速铁路轨道系统全国重点实验室，北京 100081)

摘　要：混凝土结构开裂是高原大温差环境桥墩亟待解决的关键技术难题。本工作提出了一种模拟高原昼夜温差环境的桥墩混凝土开裂试验方法，证实了声发射技术在评估混凝土内部裂缝萌生与损伤演化的可行性，揭示了大温差条件下桥墩混凝土结构的开裂机制。结果表明：大温差环境桥墩混凝土结构呈现 3 阶段损伤发展规律，即微裂缝(损伤)累积阶段、宏观开裂阶段和裂缝扩展阶段。升、降温使处于第 1 阶段和第 3 阶段桥墩混凝土结构的损伤或裂缝进一步累积和发展，而宏观开裂现象多发生于自 80~60 ℃的降温阶段，其原因是降温过程中混凝土表层收缩，但因中部仍保持膨胀状态而产生了更多损伤。同时，声发射监测数据证明，温度循环引起的疲劳拉应力是导致混凝土损伤累积和开裂的主要因素，且在温度循环过程中混凝土内部产生的拉伸裂缝占比超过 90%。

关键词：高原大温差环境；桥墩混凝土；声发射；开裂特征；损伤演变
中图分类号：U213.244　　**文献标志码**：A　　**文章编号**：0454–5648(2026)02–0719–12
网络出版时间：2026–01–07

在具有过高昼夜温差和强辐射特征的高原地区，混凝土结构在服役期间面临着更严重的开裂风险[1, 2]。在不考虑混凝土结构自身水化放热的影响下，混凝土结构在服役过程中向外界吸收的能量是导致混凝土开裂的直接原因[3–5]。表层开裂是高原大温差环境混凝土主要的破坏形式之一。高原大温差环境下，混凝土结构除因大风干燥收缩而导致开裂外，还存在因强太阳辐射和昼夜温差过大而造成结构开裂，其中桥墩等立面混凝土结构的开裂特征较为复杂，裂缝常纵横交错地分布于结构表面[6]。混凝土作为非匀质的低导热系数复合材料，结构内、外的温度梯度以及胶凝体系和骨料间的热膨胀系数差异导致的温度应力是造成结构开裂的主要原因[7–9]。本课题组[3]前期通过有限元分析了大温差环境桥墩混凝土的开裂机理，证明温度疲劳拉应力是混凝土开裂的主要原因。

现有混凝土结构检测和识别裂缝的手段包括人工目测、红外成像、数字图像相关(DIC)等技术手段[10]。人工目测方法是最直接、最简便的裂缝识别方法，但其识别精度受人为因素影响较大[11]。红外成像技术基于混凝土热传导特性通过裂缝和未损伤混凝土的导热系数差异实现裂缝识别[12]。但红外成像在测试时受环境温湿度和风速影响较大，不适合大温差环境此类气候变化大的地区[13]。数字图像相关(DIC)技术作为目前常用的图像分析手段，能够精确捕捉混凝土在荷载作用下的应变场分布特征，从而实现对裂缝的精准定位和评估[14–16]。但 DIC 技术仅是对结构表面的观测，无法捕捉混凝土内部微裂缝和损伤的发展。并且，DIC 技术对环境光线要求较高，现场实体结构的长期监测方面难以满足 DIC 设备的参数要求。

相较于其他检测/监测手段，声发射(AE)技术具备裂缝的实时捕捉、裂缝捕捉精度高、裂缝实时定位、开裂类型判定和受环境影响小等优势[17]。Radhika 等[18]采用 AE 分析技术研究了混凝土梁在静荷载和疲劳荷载作用下的断裂行为和损伤机理。Li 等[19]通过 AE 技术研究了不同疲劳应力水平下混凝土的损伤劣化规律和裂缝类型，将混凝土的疲劳破坏

收稿日期：2025–09–05。　修订日期：2025–11–12。
基金项目：国家自然科学基金(52438002；52208299)；中国铁道科学研究院集团有限公司院基金(2024YJ207)；科学探索奖 XPLORER PRIZE。
第一作者：董昊良(1999—)，男，博士研究生。
通信作者：李化建(1976—)，男，博士，研究员。

Received date: 2025–09–05.　**Revised date:** 2025–11–12.
First author: DONG Haoliang (1999–), male, Doctoral candidate.
E-mail: dhlCARS@163.com
Correspondent author: LI Huajian (1976–), male, Ph.D., Professor.
E-mail: chinasailor@163.com

过程分为 4 个阶段。Jiao 等[20]采用 AE 技术研究了钢纤维、玄武岩纤维和玻璃纤维对机制砂混凝土在荷载作用下的损伤劣化特征。但目前 AE 技术多用于测试混凝土在荷载作用下的损伤评估，尚未验证在大温差环境下混凝土结构内部的损伤监测和开裂状态评价方面的可行性。

本工作提出了一种模拟高原大温差环境桥墩混凝土开裂的试验方法，通过设置应力集中来弥补小尺寸试件在温度循环过程无法观察宏观开裂的不足。同时，采用 AE 技术实时监测、采集混凝土内部裂缝和损伤的发展规律。通过对 AE 信号参数进行分析，探明了大温差环境下桥墩混凝土结构内部损伤发展规律，探明了不同阶段桥墩混凝土结构的损伤开裂特征，揭示了桥墩混凝土结构的主要裂缝类型，证实了 AE 技术在监测和评估大温差环境下混凝土结构的可行性，以期为大温差环境混凝土结构的损伤监测及开裂评估提供参考。

1 实验

1.1 试件设计

试验使用原材料包括水泥、粗骨料、细骨料和水。水泥为 P·O 42.5 普通硅酸盐水泥，主要性能如表 1 所示。粗骨料为 5~10、10~20 mm 的连续级配碎石，主要性能如表 2 所示。细骨料为细度模数为 2.8、级配II区的天然河砂。混凝土的配合比如表 3 所示。为模拟大温差环境下桥墩混凝土结构的开裂特征，本工作设计的“内方外圆”型复合结构混凝土进行温度循环试验(图 1)。复合结构混凝土通过内部棱柱体边角位置因温度梯度作用产生应力集中现象，放大了因温度梯度引起的拉应力，这与实际桥墩结构中因截面变化、边界约束等导致的变形过程中应力集中现象具有物理相似性。通过对比应力集中部位混凝土的裂缝特征可以直观评价混凝土的抗裂性能。

表 1 水泥基本性能

Table 1 Basic properties of cement

Density/(g·cm^{-3})	Specific surface area/(m^2·kg^{-1})	Setting time/min		Flexural strength/MPa		Compressive strength/MPa	
		Initial setting time	Final setting time	3 d	28 d	3 d	28 d
3.08	364	165	235	6.2	8.9	28.3	54.6

表 2 粗骨料的主要性能

Table 2 Main properties of coarse aggregate

Apparent density/(g·cm^{-3})	Mud content/%	Mud lump content/%	Sturdiness/%	Crushing index/%	Content of needles and flakes/%	Tight clearance ratio /%	Water absorption ratio/%	14d expansion ratio/%
2.76	0.4	0.2	1	5	2	40	0.5	0.02

表 3 混凝土配合比

Table 3 Concrete mix proportion kg/m^3

Designation	Cement	Coarse aggregate		Sand	Water	SP
		10–20 mm	5–10 mm			
WC	430	785	336	604	169	1.0

WC is the designation for the concrete used in this test.

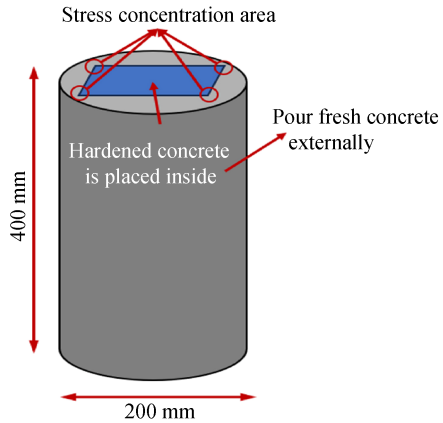


图 1 “内方外圆”型混凝土复合试件

Fig. 1 “Square inside, circle outside” type concrete composite specimen

“内方外圆”型复合结构混凝土的制备流程如图 2 所示。具体步骤如下：1) 按照配合比成型一块尺寸为 100 mm×100 mm×400 mm 的棱柱体试件并置于标准养护环境中养护 28 d；2) 将完成养护的棱柱体试件置于直径为 200 mm、高为 400 mm 的圆柱体模具的正中位置；3) 在模具中浇筑相同配合比的新拌混凝土，置于室内覆膜养护 1 d 后将试件从模具中拆除；4) 将拆除后的混凝土置于标准养护环境中养护 7 d 后取出，完成“内方外圆”型复合混凝土试件的制备。

1.2 测试设备及方法

模拟大温差环境温度循环的环境箱为深圳三思纵横科技股份有限公司生产的环境温度循环箱，能够实现–40~150 ℃温度循环的智能调控，设备的技

术要求如表 4 所示。

AE 数据采集系统采用美国 Physical Acoustics 公司生产的 Sensor Highway-III 型 AE 检测系统，AE 传感器采用 PK 15 I 集成窄带谐振传感器，谐振频率为 150 kHz，宽带频率范围为 80~200 kHz。AE 系统的详细参数设置如表 5 所示。

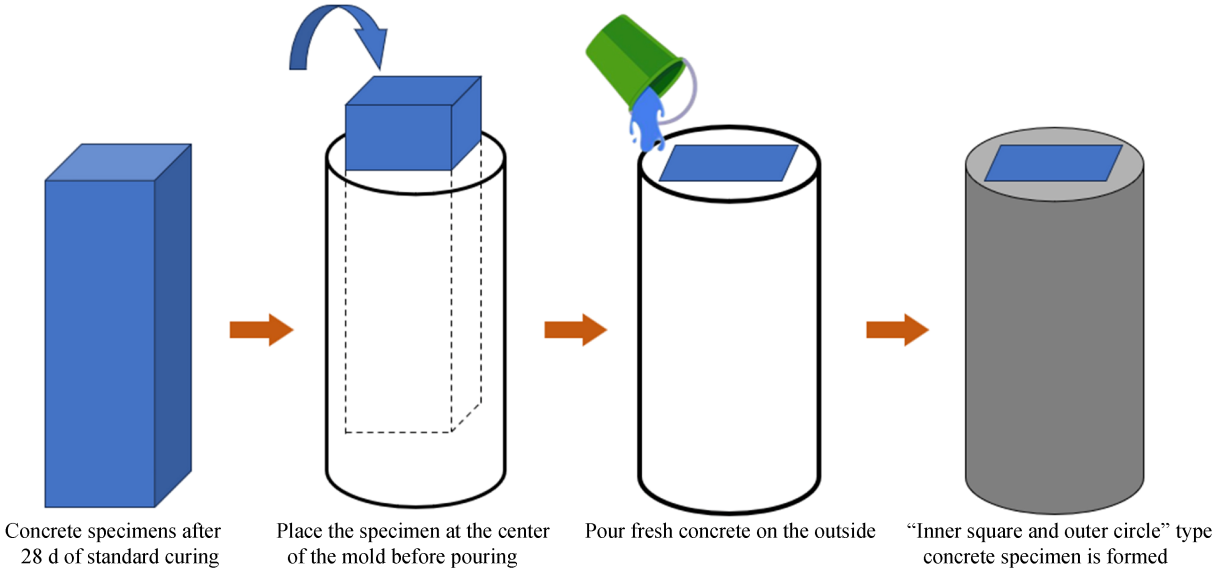


图 2　“内方外圆”型混凝土复合试件制备过程

Fig. 2　Preparation process of "square inside, circle outside" type concrete composite specimen

表 4　环境温度箱技术要求

Table 4　Environmental temperature chamber technical requirements

Parameters	Technical indicators
Available temperature range	–40–150 ℃
Heating time: From 20–150 ℃	≤60 min
Cooling time: From –40–20 ℃	≤60 min
Temperature gradient	≤2 ℃
Temperature fluctuation	≤1 ℃
Temperature deviation	≤2 ℃
Display accuracy	≤0.1 ℃
Refrigeration method	Two-stage compressor refrigeration
Heating method	Stainless steel heating tube, forced circulation air
The air circulation mode inside the box	Centrifugal fan forced circulation
Usage environment	Temperature: 5 ℃ to 35 ℃ Humidity: ≤85% Atmospheric pressure: 86 kPa to 106 kPa
Power supply	AC380 (1%±10%) V, (50±0.5) Hz, three-phase four-wire with protective ground wire

表 5　AE 系统的详细参数设置

Table 5　AE system detailed parameter settings

Parameters	Amplifier gain/dB	Threshold value/dB	Sampling rate (MSPS)	Sampling length	PDT/μs	HDT/μs	HLT/μs
Set value	26	40	1	1 k	100	200	300

MSPS means collect 10^6 points per second, with an interval of 1 μs between each two waveform points; 1 k represents 1024; PDT stands for peak definition time; HDT stands for hit definition time; HLT stands for hit latch time.

试验前，将养护 7 d 后的混凝土试件置于温度为(20±2) ℃、相对湿度为 60%±5%的恒温恒湿条件下干燥 21 d。后将混凝土试件打磨光滑并彻底清洁，以确保传感器附着效果和便于观察试件表面裂缝的发展。在圆柱体试件的侧面上、下部位各贴 8 个传感器，传感器通过耐高温硅胶耦合器与样品的界面区域耦合，传感器定位如图 3 所示。为了实现数据同步，AE 操作控制系统和温度环境箱的控制系统

同时启动和停止。

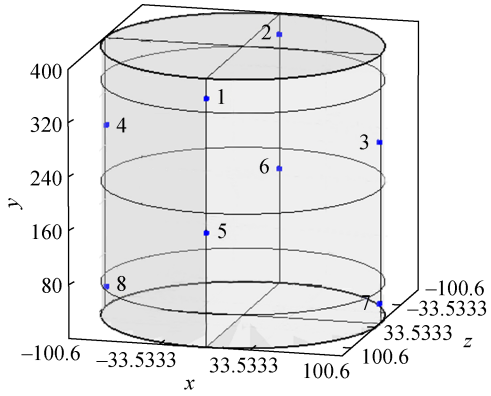


图 3 传感器安装定位

Fig. 3 Sensor installation and positioning

强太阳辐射是导致大温差环节混凝土结构白天过高温度的原因之一。Sheng 等[21]通过数值模拟发现大温差环境下混凝土结构的表面温度能够达到 61.7 ℃。文献[3]基于热传导理论计算认为高原大温差环境下混凝土结构的表面最高温度能够超过 70 ℃。且前期研究已证实，相同尺寸混凝土试件内部各个位置的温度在持续加热 2 h 后便达到加热 12 h 时相同位置温度的 85%以上。因此，为探究在极端温度循环作用下混凝土的开裂损伤演化规律，本研究设置环境箱内温度在 0~80 ℃之间循环，并以每 4 h 为一循环。本试验将标准养护 7 d 的混凝土试件在环境箱内持续进行 40 次温度循环，AE 数据采集持续时间涵盖整个温度循环周期。

1.3 AE 分析原理

AE 现象是材料或结构在外部或内部载荷作用下，伴随塑性变形或损伤演化，通过弹性波释放局部应变能的物理过程[22]。AE 检测技术通过专用仪器系统捕获此类弹性波信号，经特征参数提取与模式解析，实现对材料内部微结构演化过程的非破坏性监测[23, 24]。

固体介质发生局部变形时，同时产生体积变形与剪切变形，由此激发 2 种基本波型：纵波(压缩波)与横波(剪切波)。这些弹性波的起始位置定义为 AE 源[19]。波的传播路径呈现多模态特征，纵波与横波自激发部位向介质表面传播，部分能量被表面传感器直接接收形成基础信号；另一部分在介质表面发生折射，形成沿表面传播的瑞利波(表面波)[25, 26]。最终传感器接收的信号是多种波型在传播路径上相位干涉形成的复合信号，如图 4 所示。声波到达时序遵循纵波先至、横波次之、表面波最后的物理规律。

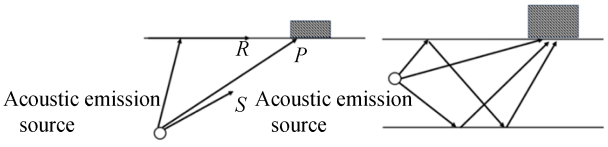


图 4 AE 技术测试原理

Fig. 4 Acoustic emission technology testing principle

1.4 AE 特征参数

AE 特征参数的定义如图 5 所示，常用的 AE 时域特征参数包括：幅值、能量、振铃计数、上升时间和持续时间等。信号的幅值通常指信号的峰值或有效值；AE 能量是指信号包络线下的面积，反映信号的强度；振铃计数是指 AE 信号中超过预设阈值电压的振荡次数的累计值；上升时间是指 AE 信号从首次超过预设阈值电压的时刻起，到达到最大振幅所需的时间间隔；持续时间是指 AE 信号从首次超过预设阈值电压的时刻起，到最终回落至阈值电压以下所需的时间间隔。作为材料或结构 AE 监测的评价标准，AE 能量还能够表征裂纹大小并评估结构的损伤程度[27, 28]。

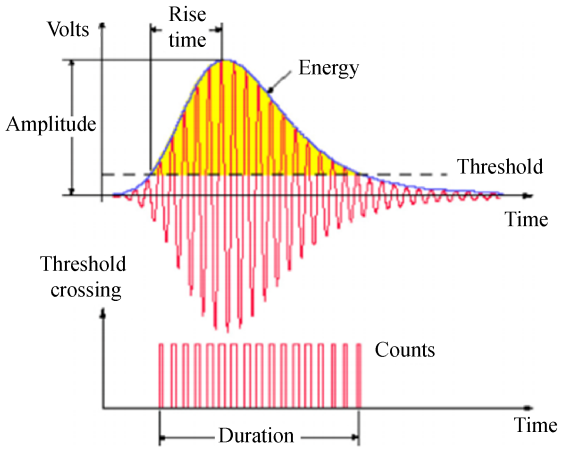


图 5 AE 的特征参数计算方法[17]

Fig. 5 AE feature parameter calculation method[17]

2 结果与分析

2.1 AE 特征参数分析

2.1.1 信号幅值 图 6 为混凝土复合试件在温度循环过程中经 AE 设备采集到的信号点及其幅值大小。由图 6 可见，在 40 次温度循环过程中，AE 设备捕捉到因混凝土应力释放或产生裂缝所输出的事件数共 539 个，且在温度循环全过程均可能出现。高幅值信号的出现说明裂缝尖端释放较高能量，通常伴随着损伤的快速累积。在温度循环过程中，大

部分 AE 信号的幅值稳定在 50~80 dB 之间，证明在温度变化产生的疲劳应力作用下，混凝土内部会因反复膨胀–收缩产生损伤，这些损伤会逐步累积并导致裂缝缓慢延伸发展。AE 信号的高幅值多出现于升温至 60~80 ℃时，证明温度循环过程中，混凝土更容易在高温环境出现损伤的快速累积或裂缝开裂。

2.1.2　信号能量　AE 能量是 AE 源释放的弹性能量，指从材料表面测得的经过传播衰减后的剩余弹性能量，多以振幅平方积分表示[29]。该参数通过量化信号包络线下的面积，反映 AE 事件的相对强度。在混凝土材料中，AE 能量与裂缝扩展程度呈正相关，能量值越高表明裂缝扩展过程中释放的弹性能量越大[30]。图 7 为温度循环过程中混凝土的信号能量分布特征，AE 信号事件数在温度循环第 16 次时出现集中增加，同时对应能量的最高值达 1943 aJ，证明此时混凝土发生了宏观开裂。同时，AE 累积能量可有效表征结构整体损伤过程。累积能量随时间急剧上升的现象与断裂过程区的形成密切相关，能量–时间曲线斜率突变可作为微裂缝合并形成宏观裂缝的判据。图 8 为温度循环过程中信号累积能量的演变规律。根据能量特征，

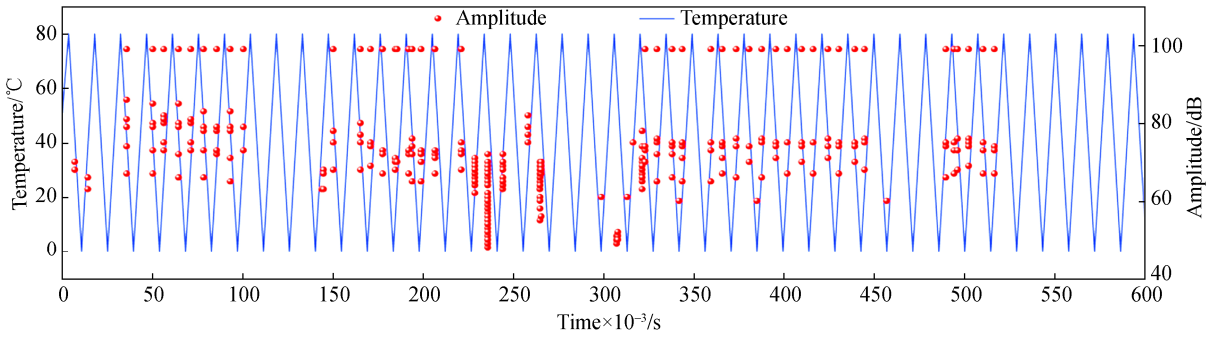


图 6　温度循环过程的信号幅值

Fig. 6　Temperature cycling process signal amplitude

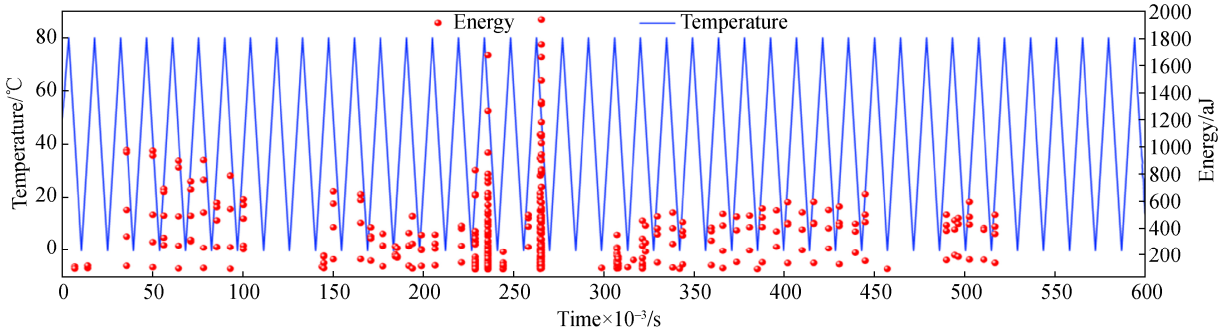


图 7　温度循环过程的信号能量

Fig. 7　Temperature cycling process signal energy

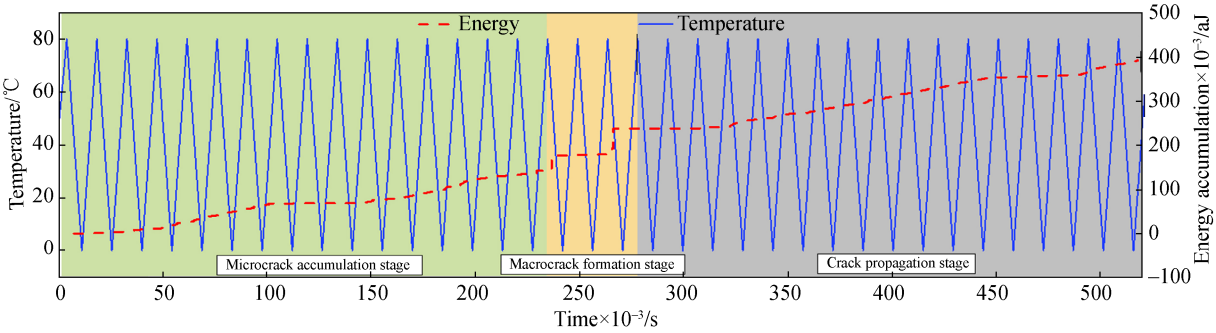
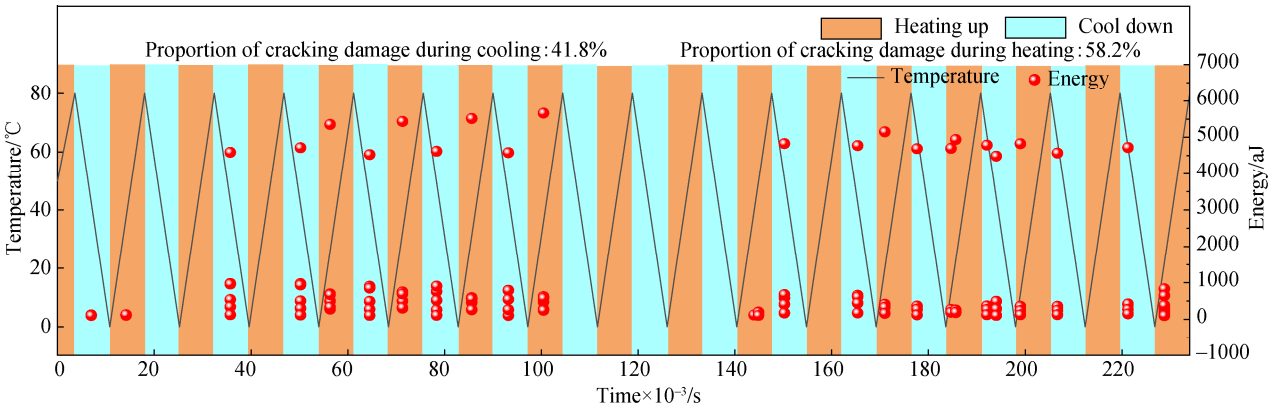


图 8　温度循环过程的能量累积

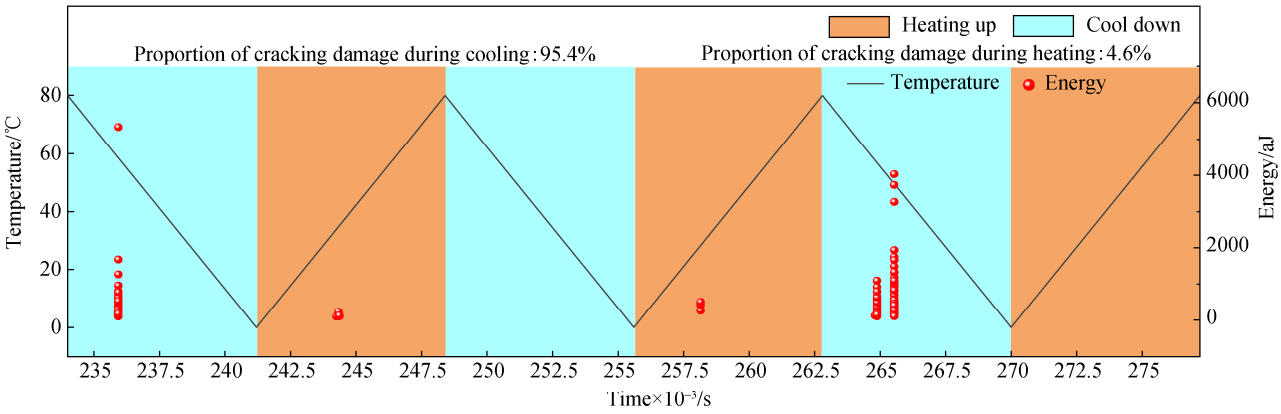
Fig. 8　Temperature cycling process energy accumulation

可将混凝土的损伤开裂过程划分为 3 个阶段：微裂缝累积阶段(前 16 次温度循环)，在温度疲劳应力作用下，混凝土内部虽未形成明显裂缝，但微裂缝持续产生并发展，表现为损伤的渐进式累积；宏观开裂阶段(第 16~19 次温度循环)，当内部损伤累积至临界值时，微裂缝贯通形成宏观裂缝，此阶段能量在短时间内快速释放，能量释放率显著增加；裂缝发展阶段(宏观裂缝形成后)，应力通过宏观裂缝释放，损伤主要集中于裂缝周边区域，能量累积过程趋于稳定，表现为裂缝的延伸扩展。

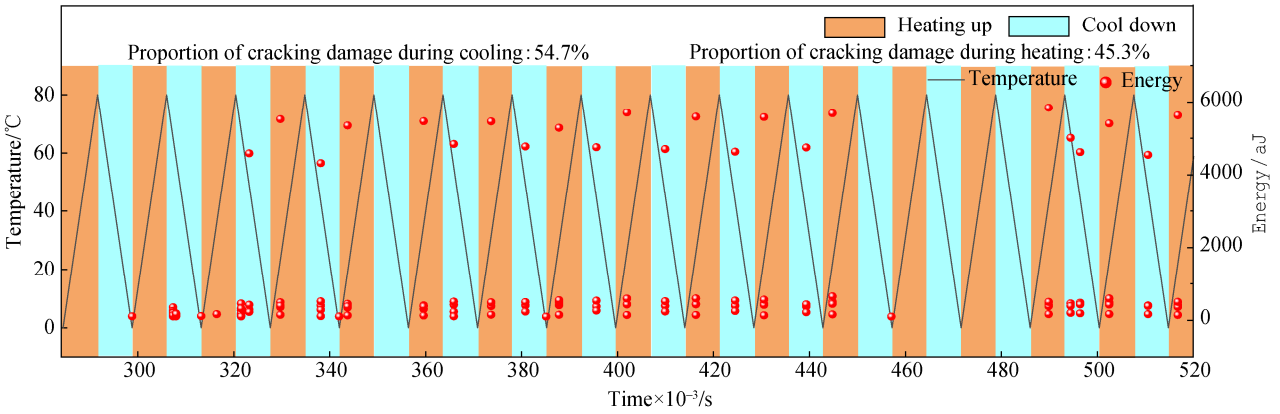
图 9 为不同阶段 AE 能量与温度的关联特征，混凝土在不同损伤阶段的温度效应存在显著差异。在微裂缝(损伤)累积阶段(第 1 阶段)和裂缝扩展阶段(第 3 阶段)，升温与降温过程引发的内部损伤或微裂缝数量呈现相近特征。具体而言，第 1 阶段中升温过程产生的 AE 信号事件数占比为 58.2%，而降温过程对应比例为 41.8%；对于第 3 阶段，升温过程的事件数占比降至 45.3%，降温过程则上升至 54.7%。值得注意的是，在宏观开裂阶段(第 2 阶段)，当环境温度从 80 ℃下降至 60 ℃时，AE 能量呈现出



(a) Temperature cycling process signal energy: Microcrack accumulation stage



(b) Temperature cycling process signal energy: Macroscopic cracking stage



(c) Temperature cycling process signal energy: Stable crack propagation stage

图 9 温度循环各阶段的信号能量

Fig. 9 Signal energy at each stage of the temperature cycling process

短时间集中大量出现的特征，其原因主要归因于温度循环过程中混凝土因反复的膨胀、收缩导致内部棱柱体拐角处而出现开裂。同时，当环境温度降低时，“内方外圆”型混凝土试件外部的温度因热量的快速散失而迅速下降，使得“内方外圆”型混凝土试件表层产生收缩，而内部则仍因具有较高温度而保持膨胀状态，使得此时混凝土尤其是薄弱部位的损伤累积速率最快[3, 31, 32]。当损伤累积达到临界值时，混凝土薄弱部位会在短时间内出现宏观裂缝，AE 数据中表现为信号能量的短时、集中出现。

2.2　AE 强度(IA)

混凝土随温度循环的损伤可通过 IA 来表征，IA 还常用于评价结构的完整性。IA 同时考虑振幅和持续时间，具体包括历史指数(HI)和严重性指数(S_r) 2 个变量[17]。IA 图通过整合 HI 与 S_r 的动态关系，实现对不同温度循环阶段混凝土的损伤程度的可视化量化。通过对数据点的分布规律，能够揭示混凝土在温度循环过程中损伤从微观到宏观的发展路径。HI 和 S_r 分别通过式(1)和式(2)进行计算。将 HI 值和 S_r 绘制的图表即为 AE 信号强度图，用于评估混凝土在温度循环过程中的受损程度[33]。

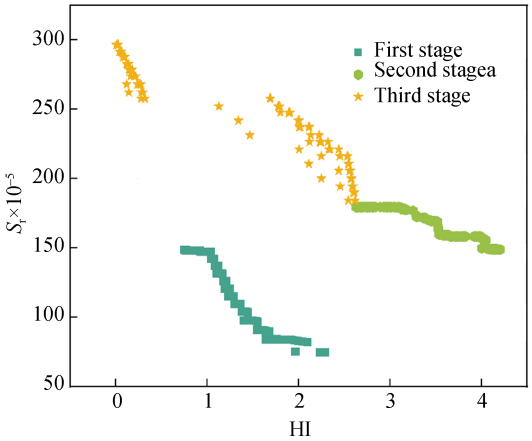
$$\mathrm{HI}(t)=\frac{N}{N-K}\frac{\sum_{i=K+1}^{N}S_{oi}}{\sum_{i=1}^{N}S_{oi}} \tag{1}$$

式中：HI(t)为时间 t 时的历史性指数；N 为截至时间 t 的 AE 事件数；K 为与材料相关的经验常数，当 $N\leqslant 50$ 时，K 取 0，当 $51\leqslant N\leqslant 200$ 时，K 取 N–30，当 $201\leqslant N\leqslant 500$ 时，K 取 0.85N，当 $N>500$ 时，K 取 N–75。；S_{oi} 为第 i 个事件的信号强度[34]。

$$S_r=\frac{1}{J}\sum_{i=1}^{J}S_{oi} \tag{2}$$

式中：S_r 为严重性指数；J 为经验常数，取信号强度最大的 J 个事件。

图 10 为温度循环过程中混凝土的 AE 强度图，随着温度循环次数的增加，混凝土的 S_r-HI 演变规律呈现标准的 3 阶段分布，从而证明基于图 10 中能量累积而得到的 3 阶段发展是准确的。在不同阶段在强度图上的数据分布产生了明显差异。第 1 阶段，温度循环作用下混凝土的 S_r 在 1.5×10^7 以内，HI 在 2.5 以内，证明这时 AE 信号的能量幅值较小，混凝土整体处于损伤不断累积的过程。但当进入第 2 阶段，温度循环作用下的 HI 迅速增加至 3.0 以上。HI 表征 AE 信号强度随时间的变化率，用于捕捉损伤发展的动态特征。HI 值的突变对应微裂缝合并为宏观裂缝的转折点，代表温度循环过程中混凝土的劣化机制从损伤的稳定累积转为裂缝失稳扩展[35–37]。而当裂缝产生后，第 3 阶段温度循环过程中混凝土的 S_r 则不断升高，且均高于 1.5×10^7，表明第 3 阶段高能量 AE 事件占比高，混凝土内部的损破坏不仅局限于损伤的累积，同时还伴随由裂缝的进一步发展。



Sr stands for severity index; HI stands for historic index.

图 10　温度循环过程混凝土的强度图

Fig. 10　Concrete strength profile in temperature cycling process

2.3　裂缝类型

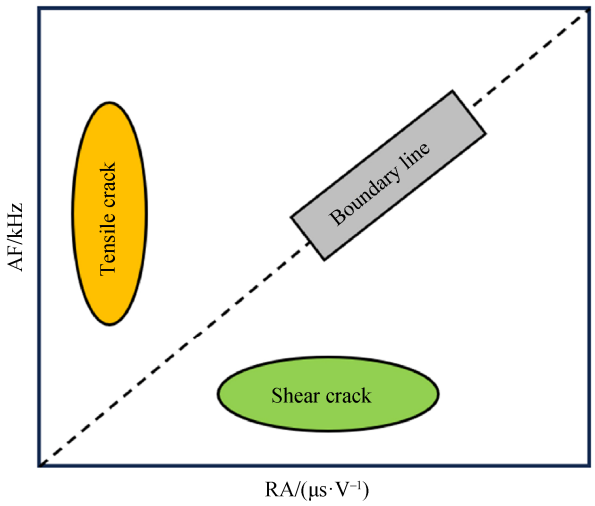
混凝土在温度循环过程产生的裂缝可分为拉伸裂缝和剪切裂缝 2 大类。研究认为，混凝土在产生拉伸裂缝时会瞬间膨胀，并以纵波(P 波)的形式释放能量；而剪切破坏则通过横波(S 波)释放能量。在波形传播的过程中，S 波的传播速度比 P 波要慢，因此，其达到峰值所需的时间更长[38]。AE 参数中，能够通过平均频率(AF)和上升角度(RA)值来识别温度循环过程中混凝土内部裂缝的类型。AF 值代表 AE 信号的频率特征，通常用于分析信号的高频或低频特性；而 RA 值则反映信号的幅度特征与上升时间之间的关系。这 2 个参数结合使用，能够更清晰地揭示裂缝在加载过程中的发展机制，从而区分拉伸裂缝和剪切裂缝的破坏模式。AF 值和 RA 值分别通过式(3)和式(4)进行计算。图 11 为采用 AF 值和 RA 值识别裂缝类型的方法。

$$\mathrm{AF}=\frac{C_{\mathrm{AE}}}{\mathrm{DUR}} \tag{3}$$

式中：C_{AE} 为振铃计数；DUR 为信号的持续时间(μs)。

$$\mathrm{RA}=\frac{\mathrm{RT}}{A_{\mathrm{AE}}} \tag{4}$$

式中：RT 为信号的上升时间(μs)；A_{AE} 为信号幅值(V)。



RA is rise angle; AF is average frequency.

图 11 AE 裂缝类型识别方法

Fig. 11 Acoustic emission crack type identification method

图 12 为“内方外圆”型混凝土试件经 40 次温度循环作用后的宏观破坏特征。由图 12 可见，试件棱柱体拐角处形成明显纵向开裂裂纹，其原因是温度循环过程中的混凝土反复膨胀和收缩导致内部棱柱体与外部混凝土之间因温度梯度产生的变形差，由此在棱柱体拐角处形成应力集中区，从而使该区域微裂缝首先贯通形成宏观裂缝。图 13 为温度循环过程中混凝土的 AF-RA 图。参考 Radhika 等[18]对混凝土裂缝类型的定义，将位于图 13 左上方的高频、低 RA 值的 AE 信号定义为拉伸裂缝，而将右下方低频、高 RA 值的 AE 信号定义为剪切裂缝。由图 13 可见，温度循环过程中混凝土内部微裂缝和



图 12 温度循环过程中混凝土的宏观开裂特征

Fig. 12 Macroscopic cracking characteristics of concrete during temperature cycling process

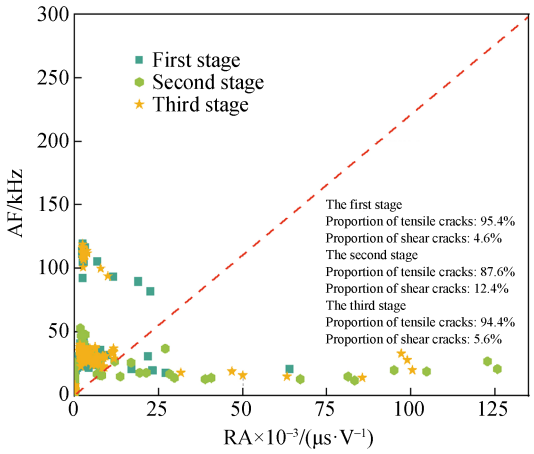


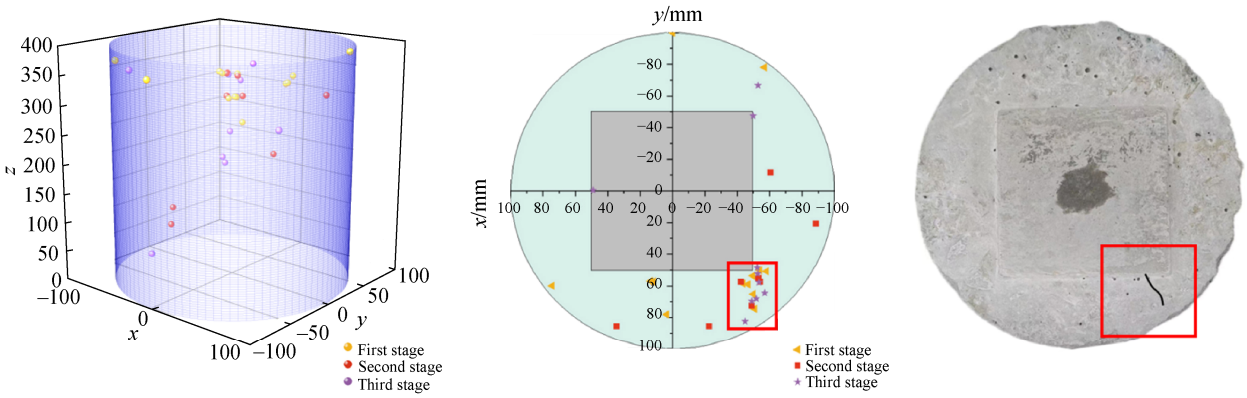
图 13 温度循环过程的裂缝类型

Fig. 13 Crack types in temperature cycling process

宏观裂缝均以拉伸开裂为主，温度疲劳拉应力作用下导致混凝土损伤或开裂的数量占总裂缝的 90%以上。第 1 阶段，混凝土内部因拉应力产生的微裂缝占总数的 95.4%，剪切裂缝仅占总数的 4.6%；第 2 阶段，混凝土内部因拉应力产生的微裂缝占总数的 87.6%，剪切裂缝仅占总数的 12.4%；第 3 阶段，混凝土内部因拉应力产生的微裂缝占总数的 94.4%，剪切裂缝仅占总数的 5.6%。由此证明，疲劳拉应力是导致大温差环境混凝土在温度循环过程中发生开裂的主要荷载类型。

2.4 裂缝定位

AE 技术能够通过弹性波传播的几何特征实现混凝土内部裂缝定位，通过捕捉混凝土内部裂缝扩展时产生的弹性波，利用传感器阵列接收信号并分析其传播特征，最终实现裂缝源的空间定位。图 14 为温度循环过程中复合结构混凝土内部的裂缝位置。由图 14 可见，因复合结构混凝土特殊的构造形式，使其在内部棱柱体混凝土边角处容易产生应力集中，从定位图亦可发现，3 个阶段的裂缝多集中于棱柱体边角的应力集中部位。在温度循环作用过程中，外部混凝土的膨胀收缩而产生的损伤率先在应力集中部位累积，并产生开裂。同时，从各阶段的裂缝发展来看，第 2、第 3 阶段的开裂位置多位于第 1 阶段的裂缝附近，证明第 2、第 3 阶段的裂缝是在第 1 阶段裂缝的基础上不断贯通、扩展产生的。同时，该结果也证明，可以使用本研究所设计的复合结构混凝土对混凝土的温度循环抗裂性进行评估，以宏观裂缝(第 2 阶段)出现所对应的温度循环次数来评估混凝土的抗裂性能。



(a) Three-dimensional positioning　　(b) Two-dimensional projection

图 14　温度循环过程的裂缝定位

Fig. 14　Crack localization in temperature cycling process

3　结论

本研究针对高原大温差环境桥墩混凝土损伤开裂问题，提出了模拟大温差环境桥墩混凝土开裂试验制度，采用 AE 技术对混凝土内部损伤发展全过程的实时监测与量化分析，揭示了大温差环境下桥墩混凝土结构开裂机理，主要结论如下：

1) 大温差环境下桥墩混凝土自温度循环初期便出现微裂缝，结构的开裂可分为微裂缝(损伤)累积、宏观开裂和裂缝扩展 3 个阶段。

2) 处于微裂缝(损伤)累积阶段和裂缝扩展阶段时，升、降温均会使桥墩混凝土的损伤或裂缝进一步累积和发展。但混凝土结构的宏观开裂多出现于从 80~60 ℃的降温阶段，其原因是降温过程中混凝土表面温度下降速率显著高于内部，桥墩混凝土内外非均匀变形导致损伤开裂。

3) 温度疲劳拉应力是大温差环境下桥墩混凝土结构开裂的主要原因，温度循环作用下混凝土的拉伸裂缝占总裂缝数量的 90%以上。同时，结构的开裂呈现沿宏观主裂缝持续损伤累积和扩展的破坏特征。

参考文献:

[1] DONG H L, LI H J, YANG Z Q, et al. Mechanical properties and constitutive model of waterborne polyurethane modified concrete in compression at different temperature[J]. J Build Eng, 2024, 98: 111357.

[2] 陈铖. 高寒高海拔地区薄壁高墩混凝土抗裂技术研究[D]. 南京: 东南大学, 2019.
CHEN Cheng. Research on crack resistance of concrete thin-walled high pier in high alpine and high altitude areas[D]. Nanjing: Southeast University, 2019.

[3] 董昊良, 李化建, 石贺男, 等. 高原大温差环境桥墩混凝土开裂机理[J]. 硅酸盐学报, 2024, 52(11): 3394–3407.
DONG Haoliang, LI Huajian, SHI Henan, et al. J Chin Ceram Soc, 2024, 52(11): 3394–3407.

[4] LU X C, CHEN B F, TIAN B, et al. A new method for hydraulic mass concrete temperature control: Design and experiment[J]. Constr Build Mater, 2021, 302: 124167.

[5] HU Y H, CHEN J, ZOU F, et al. A comparative study of temperature of mass concrete placed in August and November based on on-site measurement[J]. Case Stud Constr Mater, 2021, 15: e00694.

[6] 周有禄. 高寒地区桥墩混凝土开裂原因及修补技术应用研究[D]. 兰州: 兰州交通大学, 2014.
ZHOU Youlu. Research on cracking causes and repairing technology application of concrete piers in high altitude cold regin[D]. Lanzhou: Lanzhou Jiatong University, 2014.

[7] WANG N, LUO K, PENG K, et al. Thermal deformation and microstructure characteristics of low-heat Portland cement-based concrete in a high plateau environment[J]. J Build Eng, 2022, 58: 105025.

[8] SHEIBANY F, GHAEMIAN M. Effects of environmental action on thermal stress analysis of Karaj concrete arch dam[J]. J Eng Mech, 2006, 132(5): 532–544.

[9] DONG H L, LI H J, YANG Z Q, et al. Prediction model for fracture toughness of waterborne polyurethane modified concrete at different temperatures[J]. Constr Build Mater, 2024, 453: 139146.

[10] 董昊良, 李化建, 杨志强, 等. 高速铁路混凝土结构耐久性检(监)测与评定技术[J]. 材料导报, 2025, 39(21): 78–91.
DONG Haoliang, LI Huajian, YANG Zhiqiang, et al. Mater Rep, 2025, 39(21): 78–91.

[11] ESTES A C, FRANGOPOL D M. Updating bridge reliability based on bridge management systems visual inspection results[J]. J Bridge Eng, 2003, 8(6): 374–382.

[12] ZHENG Y X, WANG S Q, ZHANG P, et al. Application of nondestructive testing technology in quality evaluation of plain concrete and RC structures in bridge engineering: A review[J]. Buildings, 2022, 12(6): 843.

[13] CHEILAKOU E, TSOPELAS N, ANASTASOPOULOS A, et al. Strain monitoring system for steel and concrete structures[J]. Procedia Struct Integr, 2018, 10: 25–32.

[14] PAKRASHI V, BASU B, O' CONNOR A. Structural damage detection and calibration using a wavelet–kurtosis technique[J]. Eng Struct, 2007,

29(9): 2097–2108.
[15] LI H J, DONG H L, WEN J X, et al. Fracture behavior investigation of ballastless track of high-speed railway based on DIC technique[J]. Eng Fail Anal, 2024, 158: 107992.
[16] SHI H N, LI H J, HUANG F L, et al. Mechanical properties and microstructure evolution of recycled sand concrete under high-frequency flexural fatigue load[J]. J Build Eng, 2024, 97: 110885.
[17] NOORSUHADA M N. An overview on fatigue damage assessment of reinforced concrete structures with the aid of acoustic emission technique[J]. Constr Build Mater, 2016, 112: 424–439.
[18] RADHIKA V , CHANDRA KISHEN J M. A comparative study of crack growth mechanisms in concrete through acoustic emission analysis: Monotonic versus fatigue loading[J]. Constr Build Mater, 2024, 432: 136568.
[19] LI X X, MIAO T J, LIU T, et al. Acoustic emission evaluation and localization correction of concrete damage considering stress levels[J]. Case Stud Constr Mater, 2025, 22: e04281.
[20] JIAO Y B, YANG H, WANG J Y, et al. Effects of fiber properties on flexural and fracture characteristics of manufactured sand concrete based on acoustic emission[J]. J Build Eng, 2024, 84: 108308.
[21] SHENG X W, XIAO S M, ZHENG W Q, et al. Experimental and finite element investigations on hydration heat and early cracks in massive concrete piers[J]. Case Stud Constr Mater, 2023, 18: e01926.
[22] NAZARCHUK Z, SKALSKYI V, SERHIYENKO O. Acoustic Emission: Methodology and Application[M]. Cham: Springer International Publishing, 2017
[23] ABOUHUSSIEN A A, HASSAN A A A. Crack growth monitoring in fiber-reinforced self-consolidating concrete *via* acoustic emission[J]. ACI Mater J, 2019, 116(5): 181–191.
[24] ABDELRAHMAN M, ELBATANOUNY M K, ZIEHL P H. Acoustic emission based damage assessment method for prestressed concrete structures: Modified index of damage[J]. Eng Struct, 2014, 60: 258–264.
[25] ZELENYAK A M, HAMSTAD M A, SAUSE M G R. Modeling of acoustic emission signal propagation in waveguides[J]. Sensors, 2015, 15(5): 11805–11822.
[26] LIU F, GUO R, LIN X J, et al. Influence of propagation distance on characteristic parameters of acoustic emission signals in concrete materials based on low-frequency sensor[J]. Adv Civ Eng, 2022, 2022(1): 7241535.
[27] CARPINTERI A, LACIDOGNA G, ACCORNERO F, et al. Influence of damage in the acoustic emission parameters[J]. Cem Concr Compos, 2013, 44: 9–16.
[28] KHAZAEI C, HAZZARD J, CHALATURNYK R. Damage quantification of intact rocks using acoustic emission energies recorded during uniaxial compression test and discrete element modeling[J]. Comput Geotech, 2015, 67: 94–102.
[29] ZHANG P H, GUAN K, DENG W X, et al. A model for rock dissipated energy estimation based on acoustic emission measurements[J]. Front Earth Sci, 2023, 10: 1033012.
[30] LIU L, XU Y F, LIU Y, et al. Characterization of acoustic emissions from concrete based on energy activity coefficient[J]. Buildings, 2024, 14(7): 2109.
[31] ZHANG Y N, WANG S Q, HE S J, et al. Analysis of factors influencing the temperature field variation in mass concrete during hydration heat release[J]. Case Stud Therm Eng, 2023, 52: 103737.
[32] CHEN C C, CHEN S H, CHEN C C, et al. Study on temperature control and cracking risk of mass concrete sidewalls with a cooling-pipe system[J]. Buildings, 2024, 14(4): 872.
[33] SHAHIDAN S, PULIN R, MUHAMAD BUNNORI N, et al. Damage classification in reinforced concrete beam by acoustic emission signal analysis[J]. Constr Build Mater, 2013, 45: 78–86.
[34] ABOUHUSSIEN A A, HASSAN A A A, ISMAIL M K, et al. Evaluating the cracking behavior of ECC beam-column connections under cyclic loading by acoustic emission analysis[J]. Constr Build Mater, 2019, 215: 958–968.
[35] BRUNO E, SCIONTI G, CALABRESE L, et al. Intensity analysis method of acoustic emission signals for the damage monitoring of post-tensioned concrete beams[J]. Materials, 2024, 17(16): 3981.
[36] DU F Z, YANG D, LI D S, et al. Identification of damage modes and critical states for FRP/steel-concrete composite beams based on acoustic emission signal analysis[J]. Buildings, 2024, 14(8): 2378.
[37] GOSTAUTAS R S, RAMIREZ G, PETERMAN R J, et al. Acoustic emission monitoring and analysis of glass fiber-reinforced composites bridge decks[J]. J Bridge Eng, 2005, 10(6): 713–721.
[38] PREM P R, VERMA M, AMBILY P S. Damage characterization of reinforced concrete beams under different failure modes using acoustic emission[J]. Structures, 2021, 30: 174–187.

Study on Cracking Mechanism of Pier Concrete in High Altitude Large Temperature Difference Environments Based on Acoustic Emission

DONG Haoliang[1,2], *LI Huajian*[1,2], *YANG Zhiqiang*[1,2], *Huang Fali*[1,2]
(1. Railway Engineering Research Institute, China Academy of Railway Science Corporation Limited Beijing 100081, China;
2. State Key Laboratory Track Technology of High-Speed Railway, Beijing 100081, China)

Extended Abstract

Introduction In regions characterized by excessively high diurnal temperature variations and strong radiation (high-temperature-difference environments), concrete structures face heightened risks of cracking during service. Excluding the influence of hydration heat released by the concrete itself, energy absorption from the external environment during service is identified as the direct cause of concrete cracking. Surface cracking represents one of the primary failure modes for concrete in plateau regions with large temperature differences. In such environments, concrete structures are susceptible to cracking not only due to wind-induced drying shrinkage but also from intense solar radiation and excessive diurnal temperature fluctuations. Notably, vertical structures like bridge piers exhibit complex cracking patterns, with cracks often forming a crisscross network on the surface. As a non-homogeneous composite material

with low thermal conductivity, concrete experiences internal/external temperature gradients and thermal stresses arising from differences in the coefficients of thermal expansion between cementitious systems and aggregates, which constitute the principal mechanisms for structural cracking. Existing methods for detecting and identifying cracks in concrete structures include manual visual inspection, infrared thermography, and Digital Image Correlation (DIC) techniques. Manual visual inspection, while the most direct and simplest method, suffers from low accuracy due to human subjectivity. Infrared thermography identifies cracks based on thermal conductivity differences between cracked and intact concrete; however, its performance is significantly affected by ambient temperature, humidity, and wind speed, making it unsuitable for regions with dramatic climatic variations like high-temperature-difference environments. DIC, a widely used image analysis tool, precisely captures strain field distributions in concrete under load, enabling accurate crack localization and evaluation. Nevertheless, DIC is limited to surface observations and cannot monitor the development of internal micro-cracks or damage. Additionally, its stringent requirements for ambient lighting hinder its application in long-term field monitoring of actual structures.

Acoustic Emission (AE) Technology exhibits unique advantages in monitoring concrete cracking under high-temperature-difference environments. Compared to other detection/monitoring methods, AE offers real-time crack capture, high precision, crack localization, fracture type classification, and minimal environmental interference. Radhika et al. employed AE analysis to investigate fracture behavior and damage mechanisms in concrete beams under static and fatigue loads. Li et al. utilized AE to study damage degradation patterns and crack types in concrete under varying fatigue stress levels, categorizing the fatigue failure process into four stages. Jiao et al. applied AE to analyze the damage characteristics of steel fiber, basalt fiber, and glass fiber-reinforced manufactured sand concrete under load. However, current AE applications predominantly focus on damage assessment under mechanical loads, with its feasibility for internal damage monitoring and cracking state evaluation in concrete structures under high-temperature-difference environments remaining unverified.

Methods The raw materials used in this study included cement, coarse aggregates, fine aggregates, and water. The cement was P·O 42.5 ordinary Portland cement. The coarse aggregates consisted of continuous graded crushed stones with particle sizes ranging from 5 mm to 10 mm and 10 mm to 20 mm. The fine aggregates were natural river sand with a fineness modulus of 2.8 and graded in Zone II. To accelerate the simulation of concrete cracking characteristics under extreme temperature environments, a "square-inner-circle-outer" composite concrete structure was designed for temperature cycling tests. During the temperature cycling process, stress concentration induced by temperature gradients occurs at the edges and corners of the internal prismatic component, amplifying the thermal stress-induced damage to the concrete.

First, a prismatic specimen with dimensions of 100 mm × 100 mm × 400 mm was cast according to the mix design and cured in a standard curing environment for 28 d. The cured prismatic specimen was then placed at the center of a cylindrical mold with a diameter of 200 mm and a height of 400 mm. Fresh concrete with the same mix design was cast into the mold. After 1 day of indoor membrane-covered curing, the specimen was demolded and transferred to a standard curing environment for an additional 7 d, completing the preparation of the "square-inner-circle-outer" composite concrete specimen. Prior to testing, concrete specimens cured for 7 d were dried for 21 d under constant temperature and humidity conditions (20±2) ℃ and relative humidity (60±5)%. Subsequently, the specimens were polished smooth and thoroughly cleaned to ensure effective sensor adhesion and facilitate observation of surface crack development. Eight sensors were attached to both the upper and lower sections of the lateral surface of cylindrical specimens, coupled to the sample interface area using high-temperature-resistant silicone couplers. To investigate the evolution of cracking damage in concrete under extreme temperature cycling, this study set the environmental chamber temperature to cycle between 0 ℃ and 80 ℃, with each cycle lasting 4 h. Concrete specimens standardly cured for 7 d underwent 40 consecutive temperature cycles in the chamber, with AE data acquisition covering the entire duration of each temperature cycle.

Results and discussion During the 40 temperature cycles, the acoustic emission AE equipment captured a total of 539 events generated by concrete stress release or crack propagation, which occurred throughout the entire temperature cycling process. High-amplitude signals indicate intense energy release at crack tips, typically associated with rapid crack propagation or unstable cracking. Most AE signals exhibited stable amplitudes between 50 dB and 80 dB during temperature cycling, reflecting the gradual accumulation of damage and crack extension under thermal fatigue stress induced by repeated expansion-contraction cycles. High-amplitude AE signals predominantly occurred during temperature rises to 60–80 ℃, demonstrating that concrete under thermal cycling is more susceptible to rapid damage accumulation or stable crack propagation at elevated temperatures. A concentrated increase in AE event counts was observed during the 16th temperature cycle, coinciding with a peak cumulative energy of 1943 aJ, indicating significant macroscopic cracking. Furthermore, the cumulative AE energy effectively characterizes the overall structural damage process. A sharp rise in cumulative energy over time correlates with the formation of fracture process zones, and abrupt changes in the energy-time curve slope serve as a criterion for microcrack coalescence into macrocracks.

Based on energy characteristics, the concrete damage and cracking process can be divided into three stages: microcrack accumulation, macrocrack initiation, and crack propagation. After multiple temperature cycles, internal microcracks interconnect during the cooling phase due to shrinkage stresses, ultimately forming macrocracks. This phenomenon is validated by the concentrated energy release and abrupt slope changes in the cumulative energy curve during cooling. Both microcracks and macrocracks in concrete under thermal cycling are predominantly tensile in nature, with over 90% of cracks attributed to thermal fatigue tensile stresses. In summary, the composite concrete structure designed in this study can effectively evaluate the temperature cycling resistance of concrete. The number of temperature cycles corresponding to the onset of macrocracks (Stage II) serves as a

quantitative metric for assessing concrete cracking resistance.

Conclusions This paper addresses the damage and cracking of bridge pier concrete under plateau high-temperature-difference environments. A testing method simulating concrete cracking in such environments was proposed, combining AE technology to achieve real-time monitoring and quantitative analysis of internal damage evolution. The damage mechanisms under high-temperature-difference conditions were elucidated. The key conclusions are as follows: 1) Micro-cracks initiate in bridge pier concrete during the early stages of temperature cycling under high-temperature-difference environments. The cracking process can be divided into three stages: micro-crack (damage) accumulation, macroscopic cracking, and crack propagation. 2) During the micro-crack (damage) accumulation and crack propagation stages, both temperature rise and fall exacerbate damage or crack development in the concrete. However, macroscopic cracking predominantly occurs during the cooling phase from 80 ℃ to 60 ℃. This is attributed to the faster surface temperature reduction compared to the interior, creating a non-uniform deformation effect characterized by "outer shrinkage and inner expansion." 3) Temperature fatigue tensile stress is identified as the primary cause of bridge pier concrete cracking under high-temperature-difference environments. Over 90% of the total cracks observed under temperature cycling are tensile cracks. Furthermore, the failure mode exhibits continuous damage accumulation and propagation along macroscopic primary cracks.

Keywords plateau environment with large temperature differences; bridge pier concrete; acoustic emission; cracking characteristics; damage evolution